ARTICLE

Silicon Nanowires Coated with Silver Nanostructures as Ultrasensitive Interfaces for Surface-Enhanced Raman Spectroscopy

Elisabeth Galopin,[†] Jacques Barbillat,[‡] Yannick Coffinier,[†] Sabine Szunerits,[†,§] Gilles Patriarche,[||] and Rabah Boukherroub*[,†]

Institut de Recherche Interdisciplinaire (IRI, USR-CNRS 3078) and Institut d'Electronique, de Microélectronique et de Nanotechnologie (IEMN, UMR-CNRS 8520), Cité Scientifique, Avenue Poincaré - BP 60069, 59652 Villeneuve d'Ascq, France, Laboratoire de Spectrochimie Infrarouge et Raman (LASIR, UMR CNRS 8516-Bât C5), CERLA FR-CNRS 2416, Université de Lillel - Sciences et Technologies, 59655, Villeneuve d'Ascq Cedex, France, Laboratoire d'Electrochimie et de Physicochimie des Matériaux et des Interfaces (LEPMI), CNRS-INPG-UJF, 1130 rue de la piscine, BP 75, 38402 St. Martin d'Hères Cedex, France, and Laboratoire de photonique et de nanostructures (LPN, UPR-CNRS 20) Site Alcatel de Marcoussis Route de Nozay, 91460 Marcoussis, France

ABSTRACT Silver nanoparticles (Ag NPs) were chemically deposited on silicon nanowires (SiNWs), prepared using the vapor−liquid−solid (VLS) growth mechanism, using an in situ electroless metal deposition technique. The resulting SiNWs/Ag NPs composite interfaces showed large Raman scattering enhancement for rhodamine 6G (R6G) with a detection limit of 10^{-14} M and an enhancement factor of 2.3×10^8. This large enhancement factor was attributed to the presence of "hot" spots on the SiNWs/Ag NPs substrate.

KEYWORDS: silicon nanowires • silver nanoparticles • SERS • high sensitivity

1. INTRODUCTION

One of the main advantages of Raman spectroscopy over other vibrational spectroscopic techniques is the ease with which it can be used to extract valuable information from complex environments such as living tissues and cells. With the discovery of surface-enhanced Raman spectroscopy (SERS) (1), the problem of the relatively low sensitivity of Raman spectroscopy was finally overcome, and SERS is now employed as a powerful technique to obtain molecular information from chemical and biological molecules in solution and at surfaces (2−5). While the origin of SERS enhancement is still a topic of debate, two mechanisms have been proposed. The first one is based on an electromagnetic effect. The electromagnetic field at or near laser-irradiated noble metal particle surfaces is enhanced as a result of localized surface plasmon (LSPR) excitation, leading to more intense Raman scattering from molecules near or adsorbed onto the particle surface (6, 7). The SERS intensity is in this case strongly sensitive to particle size, shape, composition, arrangement, and surface structure. The second mechanism is a chemical effect, which involves specific interactions between analyte molecules and the metal particles (8, 9).

Considerable efforts have been devoted over the past few years to the preparation of SERS interfaces showing high SERS enhancement factors (EF) (10) and improved detection limits (11−14). Even though enhancement factors as high as 10^{12}−10^{14} have been reported in very particular cases (15−17), the majority of commercially available SERS interfaces exhibit an EF in the range of 10^4−10^5.

Among the different SERS interfaces examined, Ag nanoparticles from β-silver vanadate and copper and metal-decorated silica and silicon nanowires have been suggested to be effective SERS platforms (12, 18−21). Zhang et al. reported that silicon nanowires, formed by chemical etching, loaded with silver nanoparticles can be successfully used to detect immune reagents (22). Raman signals are generated with a trace amount (50 ng) of mouse immunoglobulin and its immunoreaction (22). The influence of the length of Ag-capped SiNWs, formed by chemical etching, on the Raman-enhancing capability was evaluated by Qiu et al. using a 10^{-4} M rhodamine 6G aqueous solution (20). Short and hence rigid SiNWs (<10 μm) showed large SERS intensities, while lower SERS intensities were observed for longer (>10 μm) and bent SiNWs. On the other hand, silica nanowires decorated with palladium nanoclusters, prepared by ion-implanted silicon nanowires, displayed an EF of 10^7 and a 0.1 ng mL^{-1} detection limit toward interleukin-10 (21).

Furthermore, the gold droplet catalyst used for the vapor−liquid−solid (VLS) growth of SiNWs and that resides at the top of wires has been shown to be well suited to

* To whom correspondence should be addressed. E-mail: rabah.boukherroub@iemn.univ-lille1.fr. Tel: +33 (0) 3 20 19 79 87. Fax: +33 (0) 03 20 19 78 84.
Received for review February 10, 2009 and accepted May 18, 2009
[†] Institut de Recherche Interdisciplinaire (IRI, USR-CNRS 3078) and Institut d'Electronique, de Microélectronique et de Nanotechnologie (IEMN, UMR-CNRS 8520).
[‡] Université des Sciences et Technologies de Lille.
[§] Laboratoire d'Electrochimie et de Physicochimie des Matériaux et des Interfaces (LEPMI), CNRS-INPG-UJF.
[||] Laboratoire de photonique et de nanostructures (LPN, UPR-CNRS 20) Site Alcatel de Marcoussis Route de Nozay.
DOI: 10.1021/am900087s

Published on Web 06/09/2009

exploit SERS and tip-enhanced Raman spectroscopy (TERS) effects (18). Until now, there has been, however, surprisingly no report on important SERS characteristics such as the enhancement factor and the detection limit of the VLS-grown SiNWs decorated with Ag nanoparticles.

In this work, we explore the potential of the VLS-grown SiNWs substrates capped with Ag NPs as ultrasensitive SERS interfaces. The Raman-enhancing capabilities of SiNWs/Ag NPs have been evaluated using aqueous solutions of rhodamine 6G of different concentrations.

2. EXPERIMENTAL SECTION

Materials. All cleaning (H_2O_2, 30%; H_2SO_4, 96%; HCl; HNO_3) and etching (HF, 40%) reagents were of VLSI grade and were supplied by Merck. All chemicals were reagent grade or higher and were used as received unless otherwise specified. Silver nitrate was obtained from Aldrich.

Sample Preparation. ***Silicon Nanowires Synthesis. Vapor–Liquid–Solid (VLS) Route.*** Single side polished silicon (100) oriented n-type wafers (Siltronix) (phosphorus-doped, 5–10 Ω cm resistivity) were used as substrates. The surface was first degreased in acetone and 2-propanol, rinsed with Milli-Q water, and then cleaned in a piranha solution (3/1 concentrated H_2SO_4/30% H_2O_2) for 15 min at 80 °C followed by copious rinsing with Milli-Q water. A thin layer of 4 nm of gold was thermally evaporated on the Si (100)/SiO_2 clean surface covered by a native oxide layer (13–18 Å thick). The substrate was placed in a quartz tube, which was heated in a tube furnace at 500 °C. Gold nanoparticles with a high size distribution were obtained as a result of metal dewetting on the surface. Exposure of the gold-coated surface to silane gas at a pressure of 0.133 mbar (Q = 40 sccm) at 500 °C for 60 min led to SiNWs growth (23–25).

Straight and vertically aligned silicon nanowires were grown on Si(111) substrates using the VLS technique and the following growth conditions: Q_{SiH_4}/Q_{H_2} = 12/150 sccm, T = 500 °C, P = 1.1 mbar, t = 30 min. The resulting nanowires are 2 μm in length and have 50–150 nm average diameter.

Chemical Route. Single side polished silicon (100) oriented p-type wafers (Siltronix) (boron-doped, 5–10 Ω cm resistivity) were used as substrates. The surface was first degreased in acetone and 2-propanol, rinsed with Milli-Q water, and then cleaned in a piranha solution (3/1 concentrated H_2SO_4/30% H_2O_2) for 15 min at 80 °C followed by copious rinsing with Milli-Q water. The silicon nanowires were prepared by chemical etching of the clean substrate in HF/$AgNO_3$ (5.25./0.02 M) solution at 50 °C for 10 min. The resulting surfaces were rinsed copiously with deionized water, and the silver deposits were removed using a mixture of HCl/HNO_3/H_2O (1/1/1) at room temperature (26, 27).

Safety Considerations. The H_2SO_4/H_2O_2 mixture (piranha) solution is a strong oxidant. It reacts violently with organic materials. It can cause severe skin burns. It must be handled with extreme care in a well-ventilated fume hood while wearing appropriate chemical safety protection.

HF is a hazardous acid which can result in serious tissue damage if burns are not appropriately treated. Etching of silicon should be performed in a well-ventilated fume hood with appropriate safety considerations: face shield and double-layered nitrile gloves.

Silicon Nanowire/Ag Nanoparticle Interfaces. The Ag NPs were deposited by an electroless deposition technique. The SiNWs substrate was immersed into a $AgNO_3$ (0.001 M)/HF (0.26 M) aqueous solution for 60 s, rinsed with Milli-Q water and ethanol, and then dried under a gentle stream of nitrogen.

Surface Characterization. ***Scanning Electron Microscopy (SEM).*** Scanning electron microscopy (SEM) images were obtained using an ULTRA 55 electron microscope (Zeiss, France) equipped with a thermal field emission emitter and three different detectors (EsB detector with filter grid, high-efficiency In-lens SE detector, Everhart-Thornley secondary electron detector).

Scanning Transmission Electron Microscopy (STEM), Energy Dispersive X-ray (EDX), and High Angle Annular Dark Field (HAADF). Scanning transmission electron microscopy (STEM) images were obtained using a Jeol 2200FS microscope equipped with a spherical aberration (Cs) corrector for the probe forming and a JEOL energy dispersive X-ray (EDX) system. The convergence half-angle of the electron beam was 30 mrad with a current probe of about 140 pA. The inner and outer half-angles of detection for the upper annular dark field detector (u-ADF) were 100 and 170 mrad, respectively (as is, we obtained high angle annular dark field (HAADF) images under so-called "Z contrast" conditions).

Raman Spectroscopy. The micro-Raman measurements were performed on a Labram micro-Raman spectrometer equipped with a HeNe laser (633 nm). Raman spectra were recorded by focusing the laser through a water immersion objective (Olympus, ×150, N_A = 1.25) on silicon and SiNWs/Ag NPs interfaces. The final laser power on the sample was measured and equals 8 mW. Accumulation times of 50 s were used to record the Raman spectra. The recorded spectra correspond to raw data without any correction or backgound subtraction.

3. RESULTS AND DISCUSSION

The SiNWs substrates used in this study were prepared using the VLS growth mechanism as described in our previous work (23–25). The fundamental process is based on chemical decomposition of silane gas (SiH_4) catalyzed by gold nanoparticles at high temperatures (440–540 °C). In this process, the diameter of the nanowires is determined by the diameter of the catalyst particles and, therefore, the method provides an efficient means to obtain uniform-sized nanowires. The gold nanoparticle catalysts were obtained by thermal evaporation of a thin film of gold (4 nm thick) on a clean oxidized (native oxide layer) Si (100)/SiO_2 substrate. The samples were placed into a chemical vapor deposition (CVD) furnace (quartz tube). Gold nanoparticles with a high size distribution were obtained as a result of metal dewetting at high temperatures (~500 °C) on the surface prior to SiH_4 gas injection. The silicon nanowire growth was achieved using the following parameters: gas flow 40 sccm of silane (SiH_4); P = 0.133 mbar; T = 500 °C, t = 1 h. Figure 1 shows an example of the silicon nanowires grown under these conditions. The diameter of the SiNWs is in the range 50–150 nm with a length of ~5–6 μm. The wide distribution of the nanowire size is related to the size of the gold nanoparticle catalyst formed during the dewetting of the Au film on the silicon dioxide layer at high temperatures. This behavior is common for Au nanoparticles prepared by a physical methodology, consisting of thermal evaporation of a thin Au film and its successive annealing. The silver nanoparticles (Ag NPs) on the silicon nanowire substrate were obtained by an electroless deposition technique. It consists of a simple dip of the SiNWs substrate into a $AgNO_3$ (0.001 M)/HF (0.26 M) aqueous solution for 60 s at room temperature. Figure 2 gives SEM images of the resulting SiNWs/Ag NPs hybrid structure. As can be seen from Figure 2 (left), the nanowires are homogeneously covered

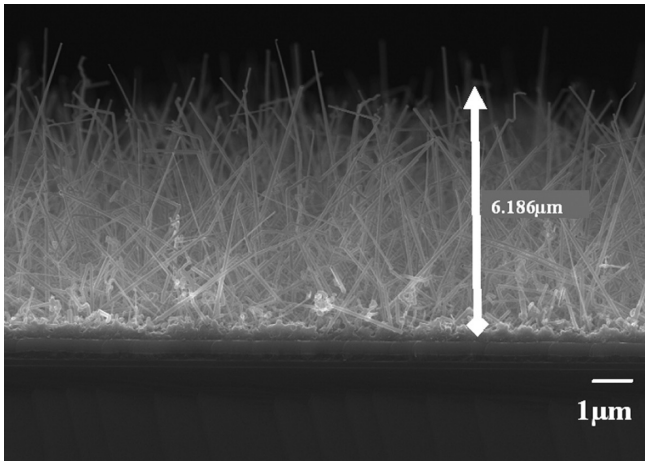

FIGURE 1. Scanning electron microscopy (SEM) image of tangled SiNWs grown by the VLS technique.

with silver nanoparticles. A high-magnification SEM image clearly indicates that the diameter of the Ag NPs deposited on the nanowires varies from 4 to 40 nm, depending on the localization on the nanowire (Figure 2, right). The largest particles, whose size ranges between 20 and 40 nm, are observed at the top of the wires, near the gold catalyst (Figure 2, Insert A). Conversely, at the bottom of the wires, the particles are smaller and flatter with an average diameter around 4 nm (Figure 2, Insert B). This could be due to the presence of dewetted gold impurities on the silicon nanowire walls (which may catalyze silver deposition) or to steric hindrance (because of the high density of silicon nanowires). Moreover, given the fast kinetics associated with the deposition reaction, it becomes hard to precisely control the nanoparticle size.

Silicon nanowire growth was performed under a reductive atmosphere; thus, freshly prepared SiNWs are hydrogen-terminated. However, upon exposure to ambient atmosphere, a native oxide layer (< 2 nm) is formed on the nanowire surface. The Ag NPs coating by an electroless deposition technique uses an aqueous solution of $AgNO_3$/HF. It is believed that HF will first dissolve the silicon dioxide native layer, allowing the reduction of Ag^+ ions into Ag^0 and thus silver nanoparticle deposition. This reduction process is balanced by silicon oxidation. The contact of Ag NPs with the SiNWs surface will form a thin oxide layer at the interface (SiNWs/Ag NPs). The presence of HF will remove the oxidized silicon bonds (Si—O—Si). Longer exposure times will lead to silicon etching and to the formation of porous silicon or silicon nanowires (26, 27). Finally, the SiNWs are oxidized spontaneously upon exposure to ambient air, leading to oxidized SiNWs coated with Ag NPs.

The SiNWs/Ag NPs interface was further characterized using scanning transmission electron microscopy (STEM). STEM characterization allows chemical contrast investigation, in contrast to HRTEM, which exploits phase contrast. Figure 3a displays a STEM image, in dark field, of a single SiNW coated with Ag NPs. At a higher magnification (Figure 3b), one clearly sees that the Ag NPs are deposited on a thin SiO_x layer. The thickness of the silicon oxide layer equals that of a native oxide layer. The STEM image (Figure 3b) also suggests the presence of gold nanoclusters on the SiNW surface. These Au nanoclusters result most likely from the gold catalyst dewetting during the SiNWs growth process and thus are directly deposited on silicon. The chemical nature of the particles was confirmed by high angle annular dark field (HAADF) contrast analysis (Figure 4). In brief, HAADF spot intensity is related to the atomic number (Z) of the nanoobject. In other words, if a small particle has HAADF contrast more intense than or equal to that of a larger particle, the two particles have different chemical compositions. Given the ratio $Z^2(\mathrm{Au})/Z^2(\mathrm{Ag}) = 2.8$, we can deduce from Figure 4 that the small particles correspond to gold

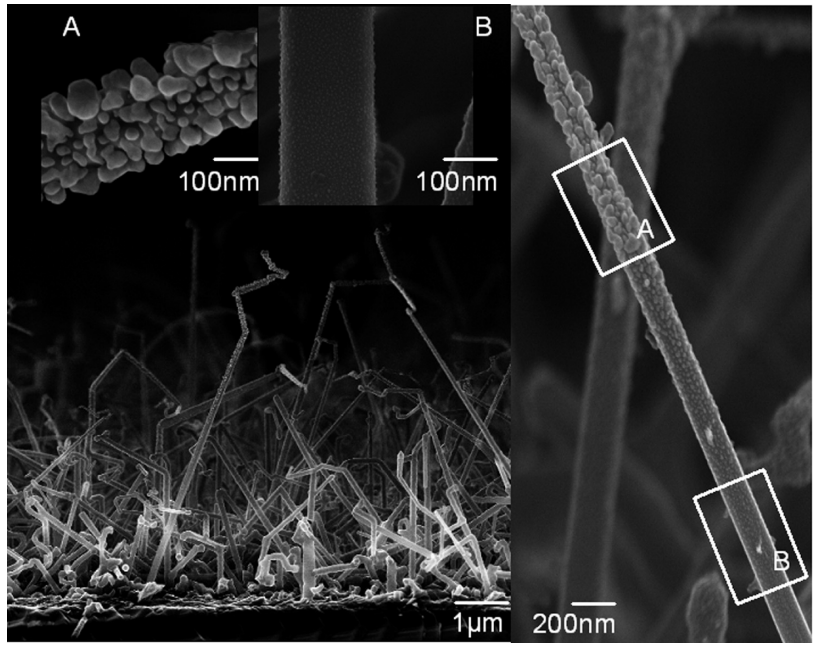

FIGURE 2. Scanning electron microscopy (SEM) images: (a) SiNWs/Ag NPs interface; (b) a single silicon nanowire decorated with Ag nanoparticles; (A, B) high-magnification images on the upper and lower parts of a SiNW/Ag NPs, respectively.

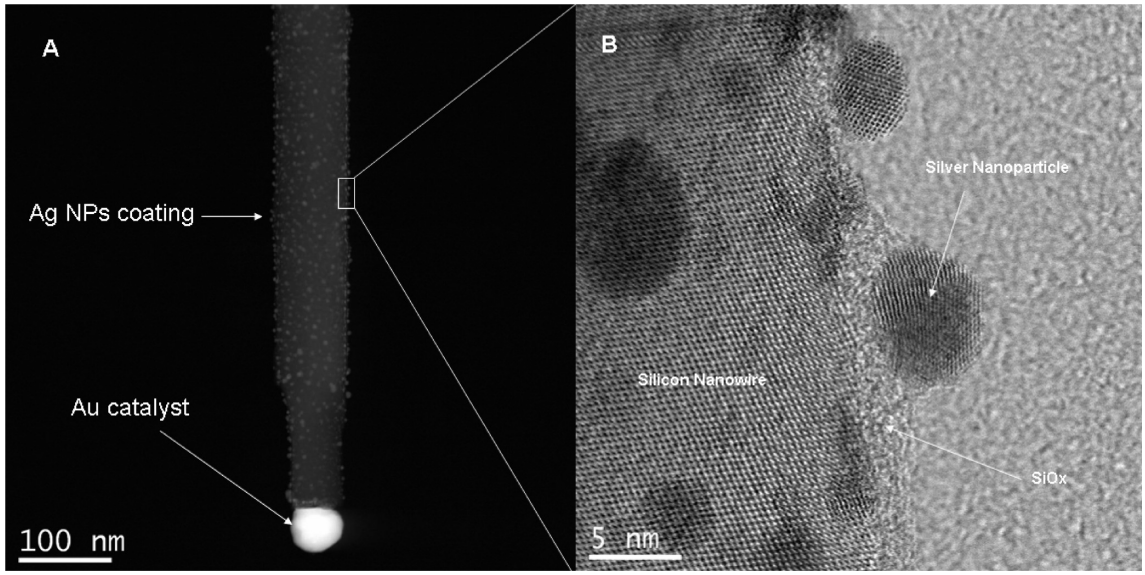

FIGURE 3. Scanning transmission electron microscopy (STEM) images: (a) in dark field, showing a single SiNW decorated with Ag NPs; (b) at a higher magnification, displaying Ag NPs deposited on a thin SiO_x layer.

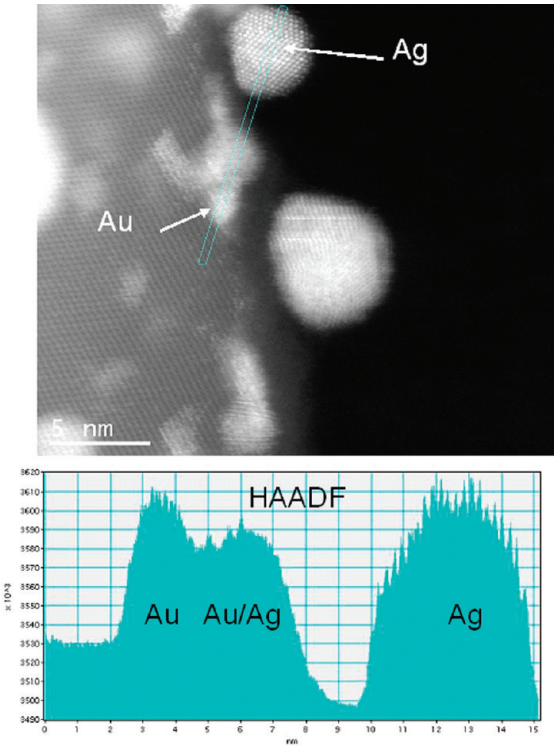

FIGURE 4. High angle annular dark field (HAADF) contrast analysis of gold nanoclusters on a single SiNW surface and Ag NPs deposited on a SiNW/SiO_x interface.

nanoclusters. The particles exhibit the same HAADF contrast as that of the particles on the SiO_x layer, but with a size 3 times smaller. We can conclude without any doubt that the NPs deposited on SiO_x are pure silver. It has to be noted that, in some cases, Ag is deposited on the gold catalyst terminating the silicon nanowires and on gold nanoclusters on the SiNWs walls. Figure 5 displays a STEM image and EDX analysis of a gold catalyst covered with Ag nanoparticles. It can be observed that Ag/Au alloy cannot be formed on small Au NPs. This is probably due to the Gibbs−Thomson effect, which creates a very strong barrier preventing the Ag

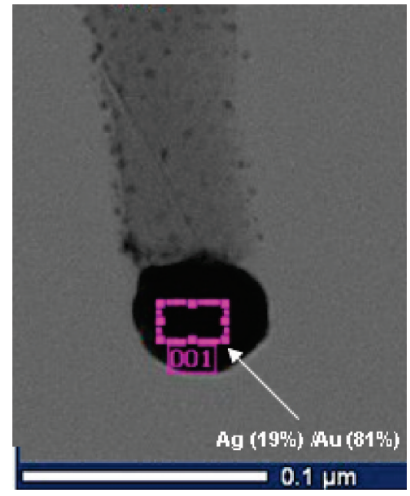

FIGURE 5. Scanning transmission electron microscopy image and EDX analysis of a gold catalyst covered with Ag nanoparticles.

diffusion inside the small Au nanoclusters. This effect can explain why larger Au NPs, as the gold catalyst, can react with Ag.

In order to evaluate the SERS capabilities of our SiNWs/Ag NPs interfaces, reference Raman spectra on SiNWs or crystalline silicon substrates (without Ag NPs) were recorded using 5 μL of an aqueous R6G solution (Figure 6). The SiNWs interface, with only gold catalyst on top, displays very weak Raman signals for a 10^{-3} M R6G aqueous solution, with a detection limit of only $\sim 10^{-4}$ M. The spectra are dominated essentially by the Si Raman peak at 520 cm^{-1} with additional weak peak patterns from 900 to 1040 cm^{-1}.

Using the same acquisition time, the SiNWs/Ag NPs interface displays clearly the spectral features of R6G at a concentration of 10^{-9} M (Figure 7). Due to the high Raman enhancement effect on the SiNWs/Ag NPs interfaces, as compared to SiNWs or crystalline silicon (without Ag NPs), a 10^{-3} M R6G aqueous solution showed saturated Raman signals on the SiNWs/Ag NPs substrates. On the SERS spectrum of a

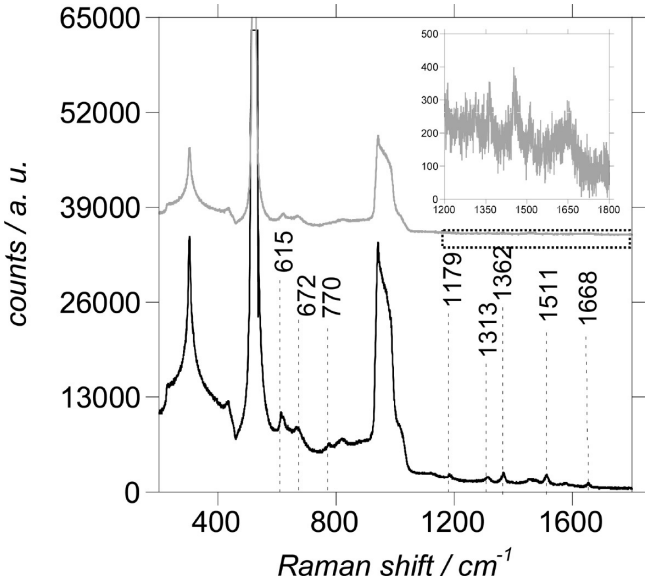

FIGURE 6. Raman spectra recorded on SiNWs substrate (without Ag NPs) covered with 5 μL of 10^{-3} M (black line) and 10^{-4} M (gray line) RG6 aqueous solution. Raman acquisition time: 50 s.

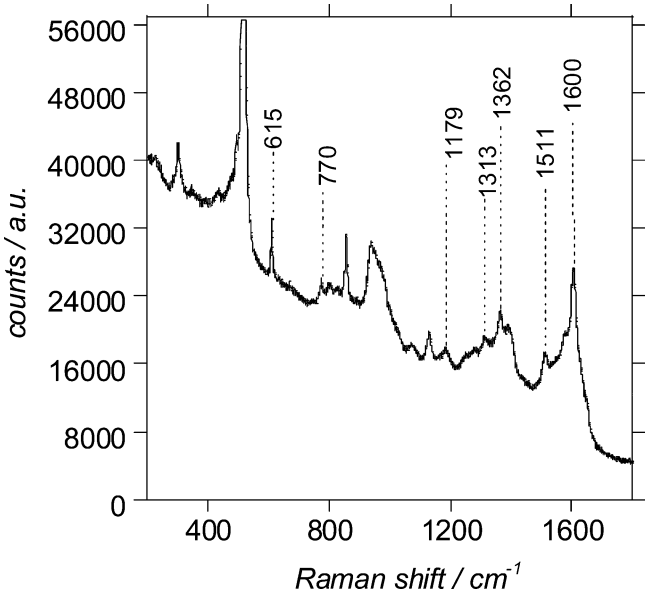

FIGURE 7. Raman spectrum recorded on a SiNWs/Ag NPs interface covered with 5 μL of 10^{-9} M R6G aqueous solution. Raman acquisition time: 50 s.

10^{-9} M R6G aqueous solution, displayed in Figure 7, some prominent bands of R6G at 1668, 1609, 1511, 1362, 1313, 1180, 770, and 615 cm^{-1} are observed (5, 20, 28, 29). The peak at 1179 cm^{-1} is associated with C−C in-plane bend modes, the signals between 1313 and 1668 cm^{-1} are attributed to aromatic C−C stretching vibrations, and the signal at 770 cm^{-1} is due to the C−H out-of-plane bend mode of R6G (12, 16). The SERS signal on the SiNWs/Ag NPs interface for a R6G concentration of 10^{-9} M is 2−40 times more intense than that of 10^{-3} M R6G on crystalline silicon or SiNWs substrates without Ag NPs. Similarly, AgNPs directly deposited on crystalline silicon substrate, using electroless deposition, exhibits a lower enhancement factor, as compared to the high aspect ratio SiNWs/Ag NPs interfaces. This clearly demonstrates the prominent role of the nanowires on the observed sensitivity. This enhancement is most likely due to the increased number of nanoparticles in the confocal volume, as compared to a flat surface. Another major contribution concerns the nanowire morphology. Indeed, the forestlike nanowires lead to a more random orientation of the nanoparticles than on flat silicon. The Raman signal is hence less influenced by the orientation and position of particles with respect to the laser polarization (18). The choice of the Raman peak has a non-negligible influence on the determination of the enhancement value. For example, the intensities under SERS and non-SERS conditions were respectively appraised at 7782 and 195 au on the basis of the 1609 cm^{-1} peak and at 2809 au and 1249 au on the basis of the 1511 cm^{-1} peak. The EF was calculated according to eq 1 (10).

$$\mathrm{EF} = \frac{I_{\mathrm{SERS}}/N_{\mathrm{surf}}}{I_{\mathrm{RS}}/N_{\mathrm{Vol}}} \tag{1}$$

with

$$N_{\mathrm{surf}} = \mu_{\mathrm{M}}\mu_{\mathrm{S}}A_{\mathrm{M}}A_{\mathrm{eff}} \tag{1a}$$

$$N_{\mathrm{vol}} = c_{\mathrm{RS}}V = c_{\mathrm{RS}}H_{\mathrm{eff}}A_{\mathrm{eff}} \tag{1b}$$

where I_{SERS} is the SERS peak intensity, I_{RS} is the non-SERS peak intensity, N_{vol} is the average number of molecules in the Raman scattering volume, N_{Surf} is the average number of adsorbed molecules in the scattering volume (V) for the SERS measurements, μ_{M} is the surface density of the individual nanostructures with respect to the main plane forming the substrate, μ_{S} is the surface density of molecules on the metal, A_{M} is the metallic surface area in each nanostructure, C_{RS} is the concentration used for the non-SERS spectra, and H_{eff} is the effective height of the scattering volume. H_{eff} was determined by following the protocol defined by Le Ru et al. (10) The axial resolution was determined by measuring the Raman intensity at 520 cm^{-1} of a silicon wafer as a function of its position along the optical axis of the 150× water immersion microscope objective. By moving the wafer above and below the focal plane, a bell-shaped curve is obtained whose FWHM (full width at half-maximum) is taken as a measure of the height of the detection volume of our microprobe. Under the conditions of use of the LabRam, we measure the effective height $H_{\mathrm{eff}} = 5.8\ \mu$m. The diameter of the laser beam focused by the 150× water immersion microscope objective of the LabRam Raman microprobe was determined by the following method (10). The intensity variation of the strong Raman line of a silicon wafer at 520 cm^{-1} was measured during a scan across the edge of a thin gold structure deposited on the Si surface. In order to accurately measure the diameter, steps of 0.1 μm were taken so that the number of points measured while crossing the edge of the metal was large enough. The simplest approach to get the diameter is by determination from the graph of intensity versus x (the displacement along the scan

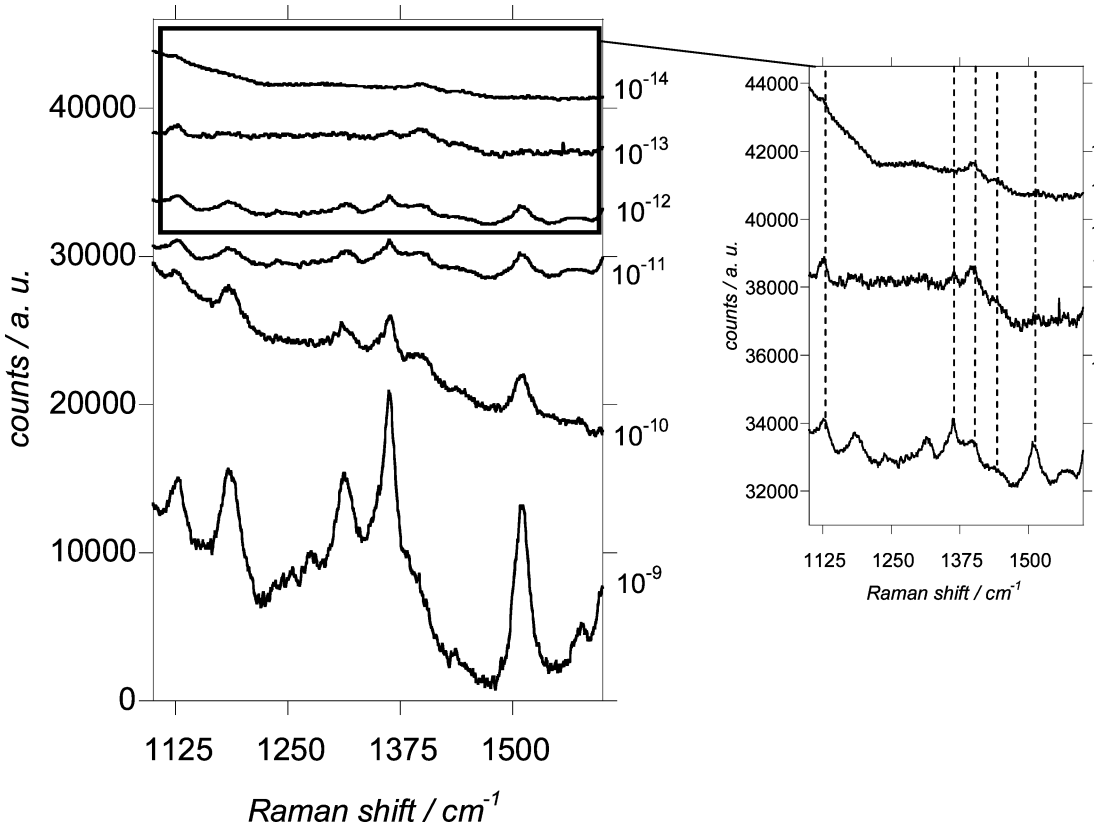

FIGURE 8. Raman spectra on SiNWs/Ag NPs interfaces covered with different concentrations of R6G. Raman conditions: acquisition time 50 s.

direction) the distance Δx for which the intensity increases from 10% to 90% of its maximum value. A beam width of 0.87 μm was determined.

This results in a final estimated scattering volume V of 3.42 μm^3 (scattering volume width 0.87 μm, section 0.59 μm^2). The length of the SiNWs, l_{SiNWs}, being $\sim$5 μm (Figure 1), in this case, $H_{eff} > l_{SiNWs}$. As the R6G solution is situated within the SiNWs, the length of the nanowire was used instead of the effective height for the calculation of the scattering volume V, which is thus $\sim$2.95 μm^3. Considering $c_{RS} = 10^{-3}$ M, N_{Vol} is then directly calculated and equals 1 775 900 molecules. From Figure 1, the mean average density of silicon nanowire can be estimated to be 10 SiNWs μm^{-2}. As we already mentioned, the Ag NPs size dispersion along the vertical direction of the nanowires makes it difficult to precisely measure the Ag NPs density. By using contrasted image treatments followed by statistical measurements, we were nonetheless able to calculate this factor. We can estimate that 75% and 25% of the surface of a single SiNW is coated with Ag nanoparticles on the upper and lower parts, respectively. The very dense and large particles (20−40 nm average diameter) occupy 30% of the wire area. Since the large particles were only present on the upper part of the nanowire, 22.5% (75 × 30) of the wire area was coated with large Ag nanoparticles. The remaining area, 17.5% (25 × 70), of the wire was covered by small particles. From these results, we can estimate that the Ag NPs occupancy is around 40% (22.5 + 17.5) on a single SiNW. Assuming a 5 μm long cylindrical nanowire of 70 nm in diameter, the surface area of the SiNWs is $\sim$1.1 μm^2. Using Ag NPs of 15 nm in diameter, this area is covered with 2490 nanoparticles. The shape of the Ag nanoparticles decorating the wire approximates a spherical cap, corresponding to half of a sphere. The metal surface area on each nanowire is $A_M \approx 1.76\,\mu m^2$, and the metal surface area in the confocal volume is $\sim$10.4 μm^2. Now assuming the contribution of a 50 nm liquid film surrounding the Ag NPs, $N_{surf} = 312 \times 10^{-3}$ molecule was determined. Note that this value, which is lower than one molecule in the confocal volume, is still sufficient to record a Raman signal. This can be explained by the molecular migration during acquisition due to Brownian motion and/or adsorption of R6G molecules on the Ag NPs (9). Depending on the choice of the Raman peak, enhancement factors (EF) from 1.2×10^7 to 2.3×10^8 under the most favorable conditions were deduced. The detection limit on the SiNWs/Ag NPs interfaces could be improved by 10 orders of magnitude from 10^{-4} to 10^{-14} M. Figure 8 shows the corresponding SERS spectra on the SiNWs/Ag NPs interfaces for R6G of different concentrations using a Raman acquisition time of 50 s. The ease with which these interfaces are formed and their good stability in aqueous solutions make the SiNWs/Ag NPs substrates interesting alternative SERS interfaces that can be used for ultrasensitive sensing (12, 14, 28).

The presence of an oxide layer did not seem to have any influence on the SERS characteristics. Indeed, Gunnarsson et al. have developed SERS interfaces using e-beam lithography for patterning Ag NPs on a SiO_2/Si substrate (30). Furthermore, Becker et al. have also shown a SERS effect on oxidized SiNWs (18). In the latter study, it was demon-

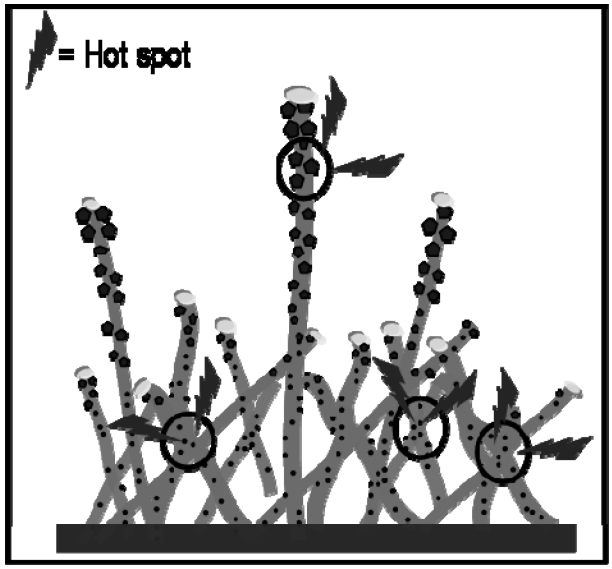

FIGURE 9. Schematic representation of potential "hot spots" on the SiNWs/Ag NPs SERS substrates.

strated that the SERS signal from silicon nanowires, synthetized via the vapor−liquid−solid (VLS) mechanism, was due notably to the presence of gold catalyst on the top of the wires and to the close-up proximity of several wires creating "hot spots" on the surface, but at high concentrations of the molecule used in their study (10^{-5} and 10^{-4} M). They have also shown that a single SiNW could give rise to a SERS signal.

It is well-documented in the literature that the large enhancement of the SERS effect is associated with the existence of "hot" spots on the SERS substrate. Hot spots where the local field enhancement is very high have been detected by searching metal nanoparticle aggregates using powerful microscopes (31, 32). The silicon nanowires investigated in this work are not well-ordered. Most of them are tangled and short, whereas some of them are long and straight. This morphology leads to the formation of "hot spots", responsible for such enormous signal amplification (EF). The presence of "hot spots" in the SiNWs/Ag NPs substrates is illustrated in Figure 9. On the basis of the substrate morphology, we can assume that "hot spots" are created at two different levels. "Hot spots" due to Ag nanoparticles, with small Ag interparticle distance, on the wires and those due to the crossing and contact between two or more silicon nanowires (tangled nanowires) (18, 33). Since the SERS spectra are averaged on a large probed confocal volume, it is believed that both types of "hot spots" contribute to the SERS signal.

The presence of hot spots was further confirmed by the observation of R6G photodecomposition products when the SERS experiments were performed at a laser power of 8 mW for longer integration times. The results are in agreement with previous reports on probing single molecules and single nanoparticles by SERS (16) and measurement of the distribution of site enhancement in SERS (34).

Finally, we have investigated the influence of SiNWs geometry on the SERS response. Straight and vertically

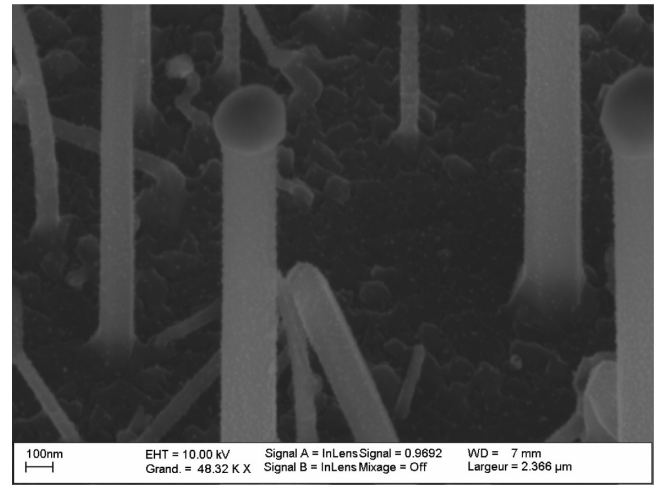

FIGURE 10. Scanning electron microscopy image of straight SiNWs prepared by the VLS technique.

aligned SiNWs 2 μm in length, with an average diameter of 50−150 nm, were prepared using the VLS technique (Figure 10). The SiNWs were coated with Ag NPs using electroless deposition from $AgNO_3$ (0.001 M)/HF (0.26 M) aqueous solution for 60 s. The resulting SiNWs/Ag NPS interfaces display a lower sensitivity than the tangled ones (from Figure 1). The SERS peak intensity at 1609 cm^{-1} was 80% lower than that obtained using the tangled nanowires. Another type of nanowire has been synthesized by chemical etching in $HF/AgNO_3$ aqueous solution (27, 28) and coated with Ag NPs. The Ag NPs were deposited using the same conditions as above. The resulting SiNWs/Ag NPs interfaces allowed a detection limit of 10^{-9} M for R6G. This clearly indicates the influence of the silicon nanowire morphology, dimension, and structure on the SERS effect. The influence of these parameters is under study.

4. CONCLUSIONS

Ultrasensitive SERS interfaces were obtained by electroless chemical coating of SiNWs, prepared by the VLS technique or by a chemical etching method, with Ag NPs. Detection limits of 10^{-14} M were recorded on SiNWs/Ag NPs composite interfaces, being several orders of magnitude more sensitive than classical Raman measurements. The SiNWs geometry plays a dominant role in the formation of "hot spots" where the local field enhancement is very important. The resonance-enhancement effect, which is present in the R6G spectra excited at 514.5 nm, may not be necessary, because surface enhancement is clearly the dominant factor (16). The high sensitivity of the SiNWs/Ag NPs interfaces is currently being exploited for the detection of biomolecular interactions.

Acknowledgment. We gratefully acknowledge the Agence Nationale de la Recherche (ANR, "LSPR project"), the Centre National de la Recherche Scientifique (CNRS), and the Nord-Pas-de Calais region for financial support.

REFERENCES AND NOTES

(1) Fleischmann, M.; Hendra, P. J.; McQuillan, A. J. *Chem. Phys. Lett.* **1974**, *26*, 163–166.

(2) Banholzer, M. J.; Millstone, J. E.; Qin, L.; Mirkin, C. A. *Chem. Soc. Rev.* **2008**, *37*, 885–897.
(3) Chourpa, I.; Lei, F. H.; Dubois, P.; Manfait, M.; Sockalingum, G. D. *Chem. Soc. Rev* **2008**, *37*, 993–1000.
(4) Pieczonka, N. P. W.; Aroca, R. F. *Chem. Soc. Rev.* **2008**, *37*, 946–954.
(5) Camden, J. P.; Dieringer, J. A.; Zhao, J.; Van Duyne, R. P. *Acc. Chem. Res.* **2008**, *41*, 1653–1661.
(6) Moskovits, M. *Top. App. Phys.* **2006**, *103*, 1–18.
(7) Lee, S. J.; Guan, Z.; Xu, H.; Moskovits, M. *J. Phys. Chem. C* **2007**, *111*, 17985–17988.
(8) Kneipp, K.; Kneipp, H., *Isr. J. Chem.* **2006**, *46*, 299–305.
(9) Sabur, A.; Havel, M.; Gogotsi, Y. *J. Raman Spectrosc.* **2008**, *39*, 61–67.
(10) Le Ru, E. C.; Blackie, E.; Meyer, M.; Etchegoin, P. G. *J. Phys. Chem. C* **2007**, *111*, 13794–13803.
(11) Grubisha, D. S.; Lipert, R. J.; Park, H.-Y.; Driskell, J.; Porter, M. D. *Anal. Chem.* **2003**, *75*, 5936–5943.
(12) Shao, M.-W.; Lu, L.; Wang, H.; Wang, S.; Zhang, M.-L.; Ma, D.-D.-D.; Lee, S.-T. *Chem. Commun.* **2008**, 2310–2312.
(13) Tan, S.; Erol, M.; Sukhishvili, S.; Du, H. *Langmuir* **2008**, *24*, 4765–4771.
(14) Liu, Y.-C.; Yu, C.-C.; Hsu, T. C. *Electrochem. Commun.* **2007**, *9*, 639–644.
(15) Chen, K.; Vo-Dinh, T., *Nanotechnol. Biol. Med.* **2007**, 16/1–16/24.
(16) Nie, S.; Emory, S. R. *Science* **1997**, *275*, 1102–1106.
(17) Kneipp, K.; Wang, Y.; Kneipp, H.; Perelman, L. T.; Itzkan, I.; Dasari, R. R.; Feld, M. S. *Phys. Rev. Lett.* **1997**, *78*, 1667.
(18) Becker, M.; Sivakov, V.; Gösele, U.; Stelzner, T.; Andrä, G.; Reich, H. J.; Hoffmann, S.; Michler, J.; Christiansen, S. H., *Small* **2008**, *4*, 398–404.
(19) Leng, W.; Yasseri, A. A.; Sharma, S.; Li, Z.; Woo, H. Y.; Vak, D.; Bazan, G. C.; Kelley, A. M. *Anal. Chem.* **2006**, *78*, 6279–6282.
(20) Qiu, T.; Wu, X. L.; Shen, J. C.; Ha, P. C. T.; Chu, P. K. *Nanotechnology* **2006**, *17*, 5769–5772.
(21) Sekhar, P. K.; Ramgir, N. S.; Bhansali, S. *J. Phys. Chem. C* **2008**, *112*, 1729–1734.
(22) Zhang, M.-L.; Yi, C.-Q.; Fan, X.; Peng, K.-Q.; Wong, N.-B.; Yang, M.-S.; Zhang, R.-Q.; Lee, S.-T. *Appl. Phys. Lett.* **2008**, *92*, 043116.
(23) Venrplanck, N.; Galopin, E.; Camart, J.-C.; Thomy, V.; Coffinier, Y.; Boukherroub, R. *Nano Lett.* **2007**, *7*, 816–817.
(24) Brunet, P.; Lapierre, F.; Thomy, V.; Coffinier, Y.; Boukherroub, R. *Langmuir* **2008**, *24*, 11203–11208.
(25) Lapierre, F.; Thomy, V.; Coffinier, Y.; Blossey, R.; Boukherroub, R. *Langmuir* **2009**, *25*, 6551–6558.
(26) Piret, G.; Coffinier, Y.; Roux, C.; Melnyk, O.; Boukherroub, R. *Langmuir* **2008**, *24*, 1670–1672.
(27) Douani, R.; Hadjersi, T.; Boukherroub, R.; Adour, L.; Manseri, A. *Appl. Surf. Sci.* **2008**, *22*, 7219–7222.
(28) Kahraman, M.; Tokman, N.; Culha, M. *ChemPhysChem* **2008**, *9*, 902–910.
(29) Hatab, N. A. A.; Oran, J. M.; Sepaniak, M. J. *ACS Nano* **2008**, *2*, 377–385.
(30) Gunnarsson, L.; Bjerneld, E. J.; Xu, H.; Petronis, S.; Kasemo, B.; Kall, M. *Appl. Phys. Lett.* **2001**, *8*, 802–804.
(31) Krug II, J. T.; Wang, G. D.; Emory, S. R.; Nie, S. *J. Am. Chem. Soc.* **1999**, *121*, 9208.
(32) Dieringer, J. A.; Lettan, R. B.; Scheidt, K. A.; van Duyne, R. P. *J. Am. Chem. Soc.* **2007**, *129*, 16249.
(33) Lee, S. J.; Morrill, A. R.; Moskovits, M. *J. Am. Chem. Soc.* **2006**, *128*, 2200.
(34) Fang, N.; Seong, N.-H.; Dlott, D. D. *Science* **2008**, *321*, 388–392.

AM900087S